Auxiliary Material for

Eastern boreal North American wildfire risk of the past 7000 years: a model-data comparison

Christelle Hély*, Martin Philippe Girardin, Adam Ahmed Ali, Christopher Carcaillet, Simon Brewer, and Yves Bergeron

*To whom correspondence should be addressed. E-mail: hely@cerege.fr

This PDF file includes:

Materials and Methods

Reconstruction of fire events: Fire events that occurred during the Holocene were reconstructed using charred particles ("charcoal") extracted from the sediments of five small kettle lakes (**Table S1; Figure S1**). One can consult *Ali et al.* [2009] for charred particle extraction and dating procedures. Based on the fact that charred area (in cm^2), charred volume (in cm^3), and charred particle counting lead to similar fire event reconstructions [*Ali et al.*, 2009], we selected the charred area (CHARa) to analyze charcoal records in the present study. To reconstruct fire events, we used methods that are described in detail by *Higuera et al.* [2007; 2008] and summarized below. First, CHARa was interpolated to constant 20-yr time steps (C$_{interpolated}$), corresponding approximately to the median temporal resolution of each record (**Table S1**). Low-frequency variations in CHARa, namely C$_{background}$, represent changes in charcoal production, transport, sedimentation, mixing, and sampling. We therefore decomposed CHARa into background (C$_{background}$) and peak (C$_{peak}$) components using a locally-defined threshold that identifies charcoal peaks likely related to the occurrence of one or more local fires (i.e. "fire events" within *ca.* one kilometer). The locally-weighted regression was applied with a 500-yr wide window that maximized a signal-to-noise (peak-to-background) index and the goodness-of-fit between the empirical and modelled C$_{background}$ distributions [*Higuera et al.*, 2009]. The residual series related to peaks was obtained by subtraction (i.e., $C_{peak} = C_{interpolated} - C_{background}$).

Consistent with theoretical evidence [*Higuera et al.*, 2007] and previous work [e.g. *Carcaillet et al.*, 2001; *Gavin et al.*, 2006; *Higuera et al.*, 2008; 2009], we assumed in the

second step that C_{peak} was composed of two subpopulations, namely $C_{noise,}$ representing variability in sediment mixing, sampling, and analytical and naturally occurring noise, and C_{fire}, representing significant peaks of charcoal input from local fires. For each peak, we used a Gaussian mixture model to identify the C_{noise} distribution. We considered the 95th, 99th, and 99.9[th] percentiles of the C_{noise} distribution as possible thresholds separating samples into "fire" and "non-fire" events, but chose the 99th percentile for simplicity and because between-record differences were similar based on all three threshold criteria. We did not screen peaks based on the original charcoal counts of each peak, as in *Higuera et al.* [2008; 2009], because this procedure is specific to charcoal counting data only. All statistical treatments were performed using the program CharAnalysis (P.E. Higuera, freely available at http://CharAnalysis.googlepages.com).

Reconstruction of fire frequency: From fire event dates extracted from C_{fire} over the past 7000 years, we computed fire frequencies (FF) using a kernel-density function [program XTREND, *Mudelsee*, 2002] that allowed a detailed inspection of time-dependent event frequencies [*Mudelsee et al.*, 2004]. In practical terms, we used a Gaussian kernel, K, to weigh observed fire event dates, $T(i)$, $i,\ldots, N$ (where N is total number of events), and calculated the frequency, *FF*, at each time *t* as:

$$FF(t) = \sum_i K((t - T(i))/h)/h$$

Selection of the bandwidth ($h = 500$ years) was guided by cross-validation aimed at finding a compromise between large variance and small bias (small *h*) and small variance and large bias (large *h*). In the case of a pooled record of multiple lakes, the values of FF are adjusted to the changing number of lake samples through time (FF') using

$FF'_{(t)} = FF_{(t)}/n_{(t)}$, where $n_{(t)}$ is the number of sampled cores at time t. We assessed the significance of changes with the help of bootstrap confidence intervals (BCI) computed from confidence bands (90%) around $FF(t)$ [*Mudelsee et al.*, 2004]. Detected trends in occurrence rate were confirmed for the measured interval using the statistical test u described by *Cox and Lewis* [1966] [also see *Girardin et al.*, 2009].

General Circulation Model data: General Circulation Models (GCMs) are time-dependent numerical representations of the atmosphere and its phenomena over the entire Earth, using the equations of motion and including radiation, photochemistry, and the transfer of heat, water vapor, and momentum. For the Holocene, the UK Universities Global Atmospheric Modelling Programme GCM [hereafter UGAMP, *Hall and Valdes*, 1997] is one of the few GCMs providing climate simulations throughout the Holocene every 1000 years (except 2000 calibrated years before present (hereafter BP) that is not available). UGAMP is an Atmosphere-slab ocean GCM. UGAMP, like all GCM simulations that are part of the PMIP 1 collection [*Joussaume and Taylor*, 2000], considers changes in the incoming solar radiation at the top of the atmosphere resulting from the long-term changes in the Earth's orbit whose parameters were prescribed following *Berger* [1978]. For UGAMP, the small changes in the atmospheric CO_2 concentration were also considered, but they accounted only for a small forcing, since the CO_2 varied between 263 and 280 ppmv during the Holocene [*Indermuhle et al.*, 1999].

GCM downscaling method: For each millenium, we computed the GCM climate anomalies (monthly means and variances) between the Holocene GCM simulation and

the present-day GCM control simulation. We considered the difference between the two periods for mean temperature, and the percentage of change for mean precipitation and for temperature and precipitation variances [*Bartlein et al.*, 1998; *Hély et al.*, 2009; *Prentice et al.*, 1998]. Significant differences among Holocene periods were found in comparing seasonal and annual temperatures or precipitation simulated by UGAMP (**Figure S2**).

We downscaled the GCM simulations to the Climate Research Unit spatial grid TS 2.1 [CRU, *Mitchell and Jones*, 2005] in order to increase the spatial resolution (from coarse GCM spatial resolutions (**Table S2**) to a finer resolution (0.5°x 0.5°)) more compatible for comparison with our local proxy records. For each climate variable, the anomaly (mean and variance) at each CRU grid point was obtained by an inverse-distance weighted average of the anomalies computed for the nearest GCM grid points. These anomalies were added to the CRU climatology to obtain the mean climate at each millennium. This type of correction [*Ramstein et al.*, 2007] only affects the mean climate, but does not alter relative changes across the region for a given period or between the different periods. When variance was not provided in GCM simulations (e.g. UGAMP), we kept the present-day observed variance computed from the CRU data set.

Within each pixel grid, we then used normal distribution for temperature and gamma distribution for precipitation [*New et al.*, 2002] to obtain a 100-year time series for each month and each variable, with each specific monthly distribution being parameterized using the reconstructed monthly mean and variance [*Ramstein et al.*, 2007]. From this 100-year time series, we ran the *Richardson* [1981] weather generator in

order to reconstruct daily temperature and precipitation necessary for the computation of the Canadian Drought Code [*van Wagner*, 1987].

Canadian Drought Code: The Canadian Drought Code (DC) is part of the Canadian Forest Fire Weather Index [FWI, *van Wagner*, 1987] used in several countries by fire agencies to predict the risk of fire ignition based on weather conditions [*de Groot et al.*, 2007]. The DC is computed on a daily [*van Wagner*, 1987] or monthly [MDC, *Girardin and Wotton*, 2009] time step, and it represents the net effect of changes in evapotranspiration and precipitation on cumulative moisture depletion in the organic matter of the deep humus layer (18-cm thick, 25 kg·m^{-2} dry weight, and 138.9 kg·m^{-3} bulk density). The daily time step calculation method of the DC was used in this study as it is the recommended option for monitoring of changes in length of the fire-season (**Figure 2D**). The scale of the DC ranges from soil saturation (zero) to extreme dryness (above 400), indicative of potential deep burning of sub-surface and heavy fuels. It is only affected by heavy rains and air temperature. It records seasonal drought with a memory of 52 days.

Daily DC calculation started every simulated year of the 100-year time series on April 1st and ended on October 31st. DC values were reset to 15 (unitless) every spring on March 31st. In order to compare the simulated DC values, we synthesized the results using monthly statistics of DC based on the 100-year daily time series for each pixel in the eastern North American region. Based on historical analysis of DC values[1], a

---

[1] http://cwfis.cfs.nrcan.gc.ca/en_CA/hamaps/fwnormals/dc

threshold of 80 units, related to moderate fire danger in the region, was used to calculate simulated fire-season length for each millennium **(Figure 2C)**. Similarly, a threshold of 160 units was used to define fire-season length under high fire danger. We computed the number of days potentially added earlier in spring or later in fall to the fire season by interpolating DC values to a daily time step. The mean DC value per month was assumed to be matched with the 15th day of each month. We counted 30 (or 31 days) for months having a mean DC value higher than the analyzed threshold (80 or 160 units), and we interpolated linearly between months for those reporting a DC mean value lower than the given threshold.

Regional averages of monthly means of DC values were determined for each month and Holocene period by averaging all pixels located within our study area. Confidence bands (90%) around DC averages were determined using the following bootstrap technique. *N* simulated events (i.e. 35 pixels, equivalent to the original sample size of the UGAMP model for our study area) were drawn with replacement and simulated DC calculated. This procedure was repeated 1,000 times, and a percentile-t confidence band was calculated. The same procedure was repeated for computation of regional averages of DC departures (anomalies) from the reference period 1901-2002 (Figure 2), except that the bootstrap procedure was applied to anomalies rather than absolute DC values. Confidence bands computed on DC anomalies tend to be slightly narrower than those obtained from absolute DC values since spatial variability (e.g. north to south and west to east gradients) originally found in absolute DC severity is removed.

Area burned, number of fires, and drought relationships: The use of DC as an indicator of fire danger potential in our study area was investigated as follows**.** Forest-fire data from the large-fire database [LFDB, *Stocks et al.*, 2003] were used to investigate the relationship between DC and fire occurrence. These large fires (size >200 ha) represent only ~3% of the fires but account for ~97% of the area burned in Canada [*Stocks et al.*, 2003]. The LFDB contains information on start location, estimated ignition date, cause, and size of each fire. Fires that occurred within the territory defined as 90-70°W and 47-55°N were compiled and time series of annual area burned (AAB) and numbers of fires (FireOcc) covering the period 1959–1997 were created. This territory was selected as fire is highly variable among years and the use of a large number of samples provided some statistical smoothing that improved the final calibration results, provided stability of the regression parameters under different divides of the calibration period [*Girardin et al.*, 2006], and minimized the prediction error. Sensitivity analyses suggested that selection of a smaller region (e.g. 83-75°W and 47-53°N) did not affect the choice of fire-predictor variable. It is worth mentioning that the quality of forest-fire statistics varies over both time and space. Even though weather/climate is the most important factor in fire activity, other factors such as changes in fire suppression, land use, ignition, and fuel can influence fire statistics [*Podur et al.*, 2002]. The area effectively under fire management is also an increasing function of time in most provinces. It is widely accepted that not all the fires that occurred in lower priority areas were detected, reported, and included in the annual fire statistics. Given these biases, it was expected that not all of the AAB and FireOcc variance would be explained by variations in the climate.

Analysis of the relationships between AAB, FireOcc, and DC was carried out using multivariate adaptive regression splines [MARS, *Friedman*, 1991] **(Figure S3)**. For the present study, fire data was regressed against monthly DC values and monthly mean temperatures from April to October over the 1959−1999 period (total of 14 potential predictor variables). MARS is a technique in which non-linear relationships between a predictand and a predictor are described by a series of linear segments of differing slopes, each of which is fitted using a basis function [*Leathwick et al.,* 2005]. Breaks between segments were defined by an inflection point in a model that initially over-fitted the data, and which was then simplified using a backward/forward stepwise cross-validation procedure to identify terms to be retained. At each step, the model selected the inflection point and its corresponding pair of basis functions that gave the greatest decrease in the residual sum of squares. Selection proceeded until some maximum model size was reached, after which a backward-pruning procedure was applied in which those basis functions that contributed least to model fit were progressively removed [*Leathwick et al.,* 2005]. The sequence of models generated from this process was then evaluated using generalized cross-validation, and the model with the best predictive fit was selected. Once the model is developed, its parameters can be applied to independent climate data (e.g. extracted from GCM simulations) for prediction of fire statistics under new conditions [*Balshi et al.*, 2009]. For other applications of MARS, one may refer to the work of *Leathwick et al.* [2005], *Balshi et al.* [2009], and *Girardin et al.* [2009]. The R package "earth" specifically developed for MARS [*Milborrow*, 2009] was used for regression.

The MARS model explained 56% of variation in FireOcc using July DC as a predictor **(Figure S3)**. The inflection point took a value of 167 units. Similarly, 37% of the variance in AAB was explained by July DC, with an inflection point estimated at 170 units. No temperature variable was selected by the model. The time lag of the DC is long enough so that July values integrate the influence of the two previous months, i.e. May and June. Over 91% of AAB (or 88% of all fires of size > 200 ha) in that area from 1959 to 1999 did so during these three months (analysis not shown). Different divisions of the calibration period also identified August DC as a potential AAB predictor. These results provide strong evidence of a link between July DC and fire activity in the area under study. One should note that previous studies have already established a strong relationship between July means of the daily DC and fire components in our area, including the work of *Girardin et al.* [2006], *Balshi et al.* [2009] and *Bergeron et al.* [2010]. In addition, the fact that similar inflection points were found in the analyses of AAB and FireOcc further strengthens the validity of using, for our study, a threshold of 160 units as an indicator of high fire risk in our area. July was selected as the reporting month of drought severity and fire risk based on these relationships.

General Circulation Models inter-comparison: In order to strengthen our confidence in the results, we compared UGAMP results to simulations from five other GCMs (**Table S2**) over the well-studied 6,000 BP time [*Joussaume and Taylor*, 2000]. For each GCM, we used the control simulation representative of the pre-industrial conditions, and assumed it was similar to present (0 BP). The region located south of Hudson Bay (**Figure S4**) was used in this comparison. It was considered as a good

compromise to be representative of eastern North America. Indeed, it encompasses several original CGM grid cells (ranging from 24 cells in IPSL to 35 cells in UGAMP, respectively) and its fire return interval is assumed to have a regional uniformity due to the homogeneity of its environment in terms of vegetation and topography. Sensitivity analyses suggested that selection of an even smaller region did not affect the results. The simulated mean Drought Code values for July at 6000 BP were statistically compared among GCMs using parametric one-way analysis of variance. Results showed no significant difference among GCMs **(Figure S4)**, which strengthened us in using UGAMP simulations through the Holocene analysis.

Fire-independent climate proxies: We used several independent climate proxies available for eastern North America to reconstruct the Holocene climate over the region and for comparison with UGAMP simulations and fire-frequency (FF) reconstructions.

Estimates of the residual Laurentide Ice-Sheet (LIS) areas (**Figure S5**) are deduced from maps by *Dyke et al.* [2003] available on the Web site of Natural Resources Canada (http://sst.rncan.gc.ca/ercc-rrcc/proj4/theme1/act1_f.php). Maps whose ages are in ^{14}C cal yr BP were first calibrated and then transferred into a GIS to estimate the LIS area, millennium after millennium. The LIS areas were estimated for eastern Canada covering northeastern Ontario, the whole Quebec-Labrador peninsula, the Canadian Maritime provinces, Newfoundland, and the northern part of New England in the United States (**Figure S5**). The LIS areas decreased from 13,000 BP (~2,900,000 km^2) to 5000 BP when it had completely disappeared. At 7,000 BP, the residual LIS still covered ~200,000 km^2 in northern Quebec-Labrador peninsula.

Reconstruction of July air temperature (**Figure 3C**) based on pollen series are available for southern Quebec [*Muller et al.*, 2003], eastern James Bay [*Kerwin et al.*, 2004], northern Quebec [*Viau and Gajewski*, 2009] and, from larger data sets, for eastern Canada [*Viau et al.*, 2006]. These reconstructions are based on the modern-analogue technique [*Overpeck et al.*, 1985]. The available temperature anomaly reconstructions differ little, and the fluctuations of temperatures since 5,000 BP are small. The main differences in July temperature among the reconstructions are observed before 5,500 BP. The southern reconstruction [*Muller et al.*, 2003] indicates higher temperature anomalies than present, whereas the other reconstructions, all from the north, display nil-to-negative July temperature anomalies [*Kerwin et al.*, 2004; *Viau et al.*, 2006; *Viau and Gajewski*, 2009].

Annual precipitation reconstructions (**Figure 3D**), inferred from pollen data, are available for only two studies: southern Quebec [*Muller et al.*, 2003] and northern Quebec [*Viau and Gajewski*, 2009]. Both reconstructions indicate drier conditions than present before 4,000 BP (the northern region displays less dry conditions than the southern region), whereas they diverge between 3,000 and 1,000 BP, with the northern reconstruction indicating wetter conditions than present.

Reconstructions of dryness (**Figure 3E**) are based on lake-level status inferred from several proxies including biological remains, and sedimentary and geomorphic evidence. Lake-level status (relative to present) is reconstructed for individual lakes, and then the lake statuses from a particular area are accumulated to determine the regional lake-level status. All studies performed in Ontario and Quebec were plotted in **Figure 3E** from north to south as follows: *a*: *Payette and Filion* [1993], *b*: *Miousse et al.* [2003], *c*:

Moos et al. [2009], ***d***: *Lavoie and Richard* [2000], ***e***: *Muller et al.* [2003], ***f***: *Yu et al.* [1996], ***g***: *Yu and McAndrews* [1994], ***h***: *Yu et al.* [1997]. The lake levels were predominantly low between 7,000 and 3,200 BP, especially from 5,000 to 3,500 BP, and higher since 3,000 BP, suggesting most likely an increase in precipitation, or possibly a decrease in evaporation or an increase in P-E, with all these conditions being less favorable to fire occurrence. Although lake level depends on long-term annual precipitation variability much more than temperature and insolation [*Harrison et al.*, 1993], a European study showed that the winter run-off is the dominant process that controls the water-table fluctuations in northern latitudes [*Vassiljev et al.*, 1998].

Auxiliary Tables

Table S1. Main characteristics of the five kettle lakes and sampled sediment cores.

	Lac aux Geais	Lac Profond	Lac Raynald	Lac à la Loutre	Lac à la Pessière
Latitude	49°53'32.2"N	49°51'40.1" N	49°48'33.4" N	49°42'42.1" N	49°30'30.0"N
Longitude	78°39'18.4" W	78°36'47.9" W	78°32'09.0" W	78°20'09.0" W	79°14'25.0" W
Elevation m (a.s.l.)	280	270	250	274	305
Local vegetation	*Picea mariana,* *Abies balsamea* *Larix laricina* *Betula papyrifera*	*Picea mariana* *Abies balsamea* *Betula papyrifera*	*Picea mariana* *Picea glauca* *Abies balsamea* *Larix laricina* *Betula papyrifera*	*Picea mariana* *Larix laricina* *Abies balsamea*	*Picea mariana* *Abies balsamea* *Larix laricina*

	Pinus banksiana				
Hill slope	Flat	Flat	Moderate	Flat	Flat
Lake surface (ha)	3.6	0.6	1.5	2.1	4
Water depth (m)	10.2	> 20	10.3	10.6	16.0
Length of organic core (cm)	603	223	472	227	302
Mean deposition time (SE) yr/cm	$13.2 \pm (0.35)$	$18.3 \pm (0.50)$	$15.2 \pm (0.30)$	$36.6 \pm (0.76)$	$13.0 \pm (0.11)$

Table S2. General Circulation Model characteristics and simulated July Drought Code for 6000 cal yr BP.

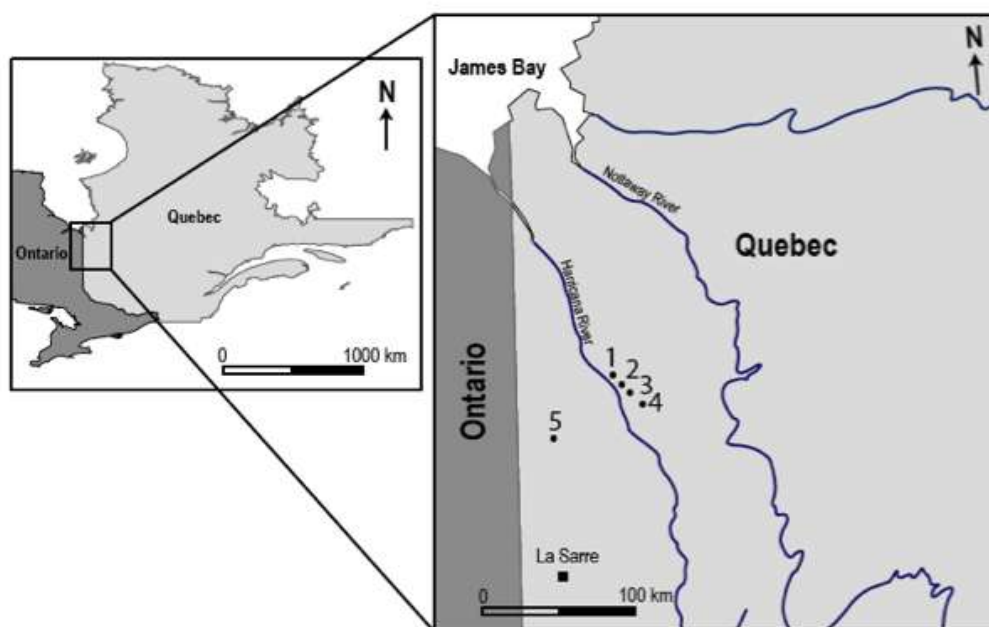| MODEL	RESOLUTION Atm. Long x Lat (*levels*)	REFERENCE	JULY DC (Mean $\pm$ SD)
CCSM3	T42 (~ 2.8° x 2.8°) (*26*)	[*Collins et al.*, 2006]	149 ± 33
FOAM	R15 (40 lat x 48 long) (*18*)	[*Jacob et al.*, 2001]	168 ± 38
FGOALS-g1.0	T42 (~ 2.8° x 2.8°) (*26*)	[*Yu et al.*, 2002]	160 ± 29
IPSL-CM4 -V1-MR	3.75°×2.5° (*19*)	[*Marti et al.*, 2005]	167 ± 37
UBRIS-HadCM3M2	3.75°×2.5° (*19*)	[*Gordon et al.*, 2000]	159 ± 34
UGAMP	T42 (~ 2.8° x 2.8°) (*19*)	[*Slingo et al.*, 1994]	178 ± 44

Auxiliary Figures

Figure S1. Location of the eastern North American region with the five kettle lakes shown. 1: Lac aux Geais; 2: Lac Profond; 3: Lac Raynald; 4: Lac à la Loutre; 5: Lac à la Pessière.
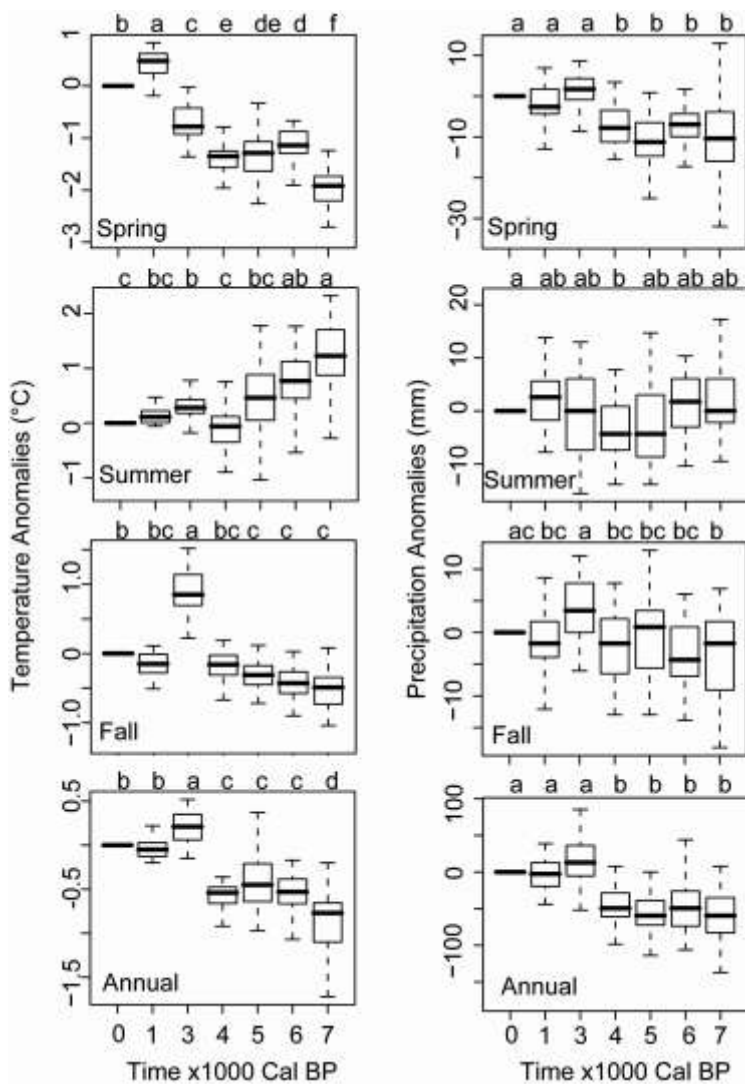
Figure S2. Seasonal and annual multiple comparisons among millennia, from 7,000 BP to present (no 2,000 BP simulation). One Tukey range test was performed for each season (spring, summer, and autumn), annual temperature anomalies in left column and precipitation in right column, respectively. All tests used n = 245 (35 original pixels from the UGAMP model and 7 millennia), df = 6, and computed p-values were less than 0.0001 for all panels, except summer precipitation (p-value < 0.002). In a given subplot, millennia with different letters are significantly different.
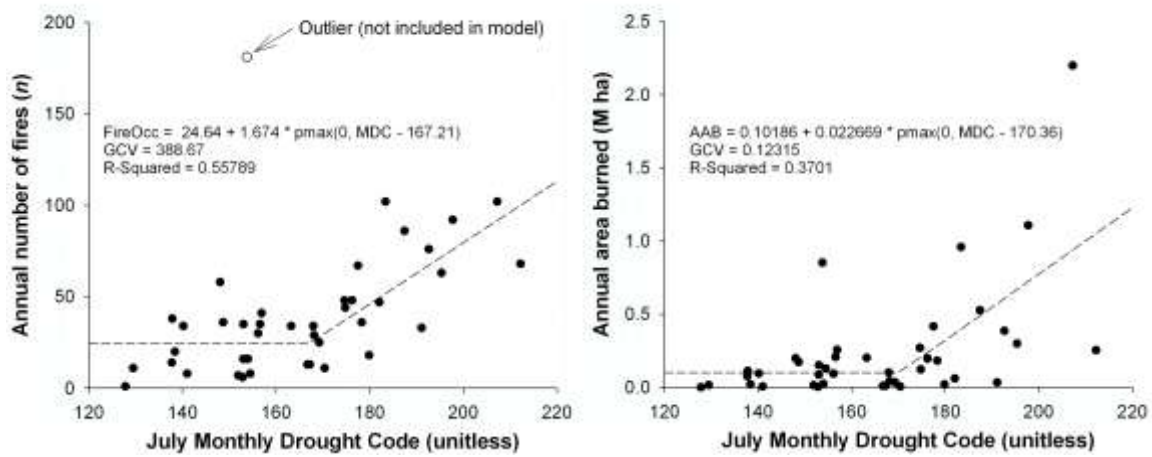
Figure S3. Relationships between the July monthly drought code, number of fires (FireOcc, left subfigure) and annual area burned (AAB, right subfigure) modeled using Multivariate Adaptive Regression Splines.
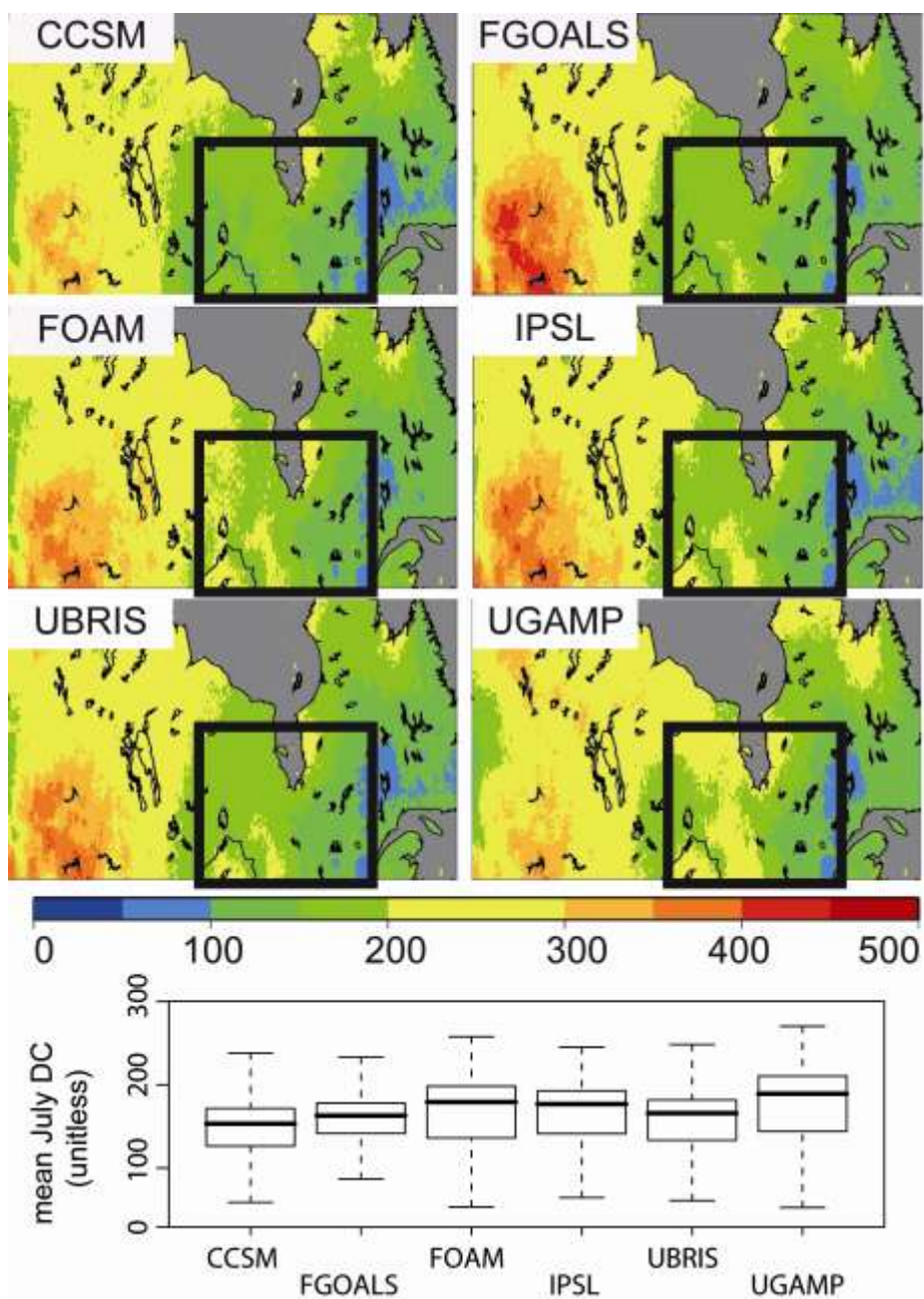
Figure S4. Spatial distribution of the mean Drought Code values simulated for July at

6,000 cal yr BP by six GCM (**Table S2**). The mean comparison test (boxplots), based on

the restricted region (90-70°W and 47-55°N, back frame on maps) showed no significant difference among GCMs (one-way ANOVA, F = 1.851, df = 153, $p > 0.05$).
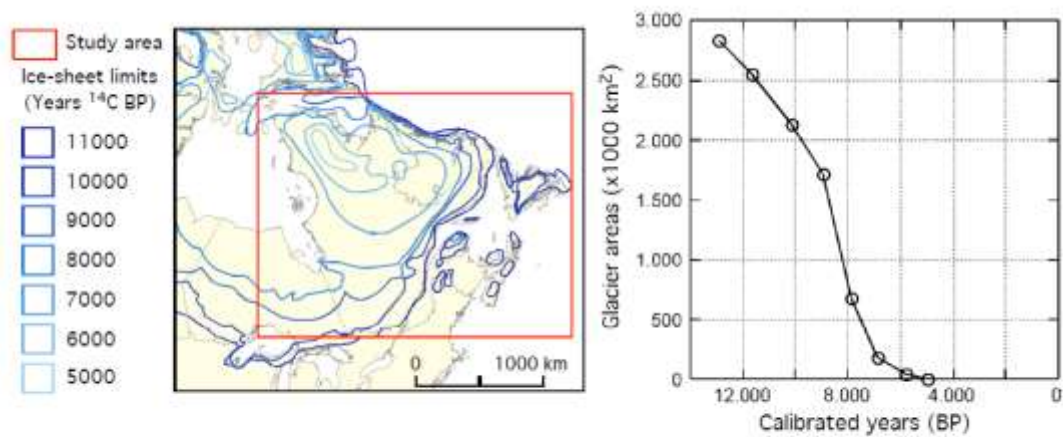

Figure S5. Laurentide Ice-Sheet areas plotted against time (cal yr BP). The region where the glacier areas were assessed is found within the red delimited zone. The glacier limits are displayed by dark blue (11,000 ^{14}C BP) to light blue lines (5,000 ^{14}C BP). Data from *Dyke et al.* [2003].

References

Ali, A. A., P. E. Higuera, Y. Bergeron, and C. Carcaillet (2009), Comparing fire-history interpretations based on area, number and estimated volume of macroscopic charcoal in lake sediments, *Quaternary Research*, *72*, 462-468.

Balshi, M. S., A. D. McGuire, P. Duffy, M. Flannigan, J. Walsh, and J. Melillo (2009), Assessing the response of area burned to changing climate in western boreal North America using a Multivariate Adaptive Regression Splines (MARS) approach, *Global Change Biology*, *15*, 578-600.

Bartlein, P. J., K. H. Anderson, P. M. Anderson, M. E. Edwards, C. J. Mock, R. S. Thompson, R. S. Webb, T. Webb III, and C. Whitlock (1998), Paleoclimate simulations for North America over the past 21,000 years: features of the simulated climate and comparisons with paleoenvironmental data, *Quaternary Science Reviews*, *17*, 549-585.

Berger, A. L. (1978), Long-term variations of daily insolation and quaternary climatic changes, *Journal of the Atmospheric Sciences*, *35*, 2362-2367.

Carcaillet, C., Y. Bergeron, P. J. H. Richard, B. Fréchette, S. Gauthier, and Y. T. Prairie (2001), Change of fire frequency in the eastern Canadian boreal forests during the Holocene: does vegetation composition or climate trigger the fire regime? *Journal of Ecology*, *89*, 930-946.

Collins, W. D., M. L. Blackmon, G. B. Bonan, J. J. Hack, T. B. Henderson, J. T. Kiehl, W. G. Large, and D. S. McKenna (2006), The Community Climate System Model Version 3 (CCSM3), *Journal of Climate*, *19*, 2122-2143.

Cox, D. R., and P. A. W. Lewis (1966), *The Statistical Analysis of Series of Events*, John Wiley and Sons Inc., New York.

de Groot, W. J., R. D. Field, M. A. Brady, O. Roswintiarti, and M. Mohamad (2007), Development of the Indonesian and Malaysian Fire Danger Rating Systems, *Mitigation and Adaptation Strategies for Global Change*, *12*, 165-180.

Dyke, A. S., A. Moore, and L. Robertson (2003), *Deglaciation of North America*. [computer file], Geological Survey of Canada, Open File 1574, Natural resources Canada, Ottawa, ON.

Friedman, J. H. (1991), Multivariate adaptive regression splines, *Annals of Statistics*, *19*, 1-67.

Gavin, D. G., F. S. Hu, K. Lertzman, and P. Corbett (2006), Weak climatic control of stand-scale fire history during the late Holocene, *Ecology*, *87*, 1722-1732.

Girardin, M. P., Y. Bergeron, J. C. Tardif, S. Gauthier, M. D. Flannigan, and M. Mudelsee (2006), A 229-year dendroclimatic-inferred record of annual forest fire activity for the Boreal Shield of Canada, *International Journal of Wildland Fire*, *15*, 375-388.

Girardin, M. P., J. C. Tardif, B. Epp, and F. Conciatori (2009), Frequency of cool summers in interior North America over the past three centuries, *Geophysical Research Letters*, *36*, L07705, doi:10.1029/2009GL037242.

Girardin, M. P., and B. M. Wotton (2009), Summer moisture and wildfire risks across Canada, *Journal of Applied Meteorology and Climatology*, *48*, 517-533.

Gordon, C., C. Cooper, C. A. Senior, H. Banks, J. M. Gregory, T. C. Johns, J. F. B. Mitchell, and R. A. Wood (2000), The simulation od SST, sea ice extents and ocean heat transports in a version of the Hadley Centre coupled model without flux adjustement, *Climate Dynamics*, *16*, 147-168.

Hall, N. M. J., and P. J. Valdes (1997), A GCM simulation of the climate 6000 years ago, *Journal of Climate*, *10*, 3-17.

Harrison, S. P., I. C. Prentice, and J. Guiot (1993), Climatic controls of Holocene lake-level changes in Europe, *Climate Dynamics*, *8*, 189-200.

Hély, C., P. Braconnot, J. Watrin, and W. Zheng (2009), Climate and vegetation: Simulating the African humid period, *Comptes Rendus Géoscience*, *341*, 671-688.

Higuera, P. E., M. E. Peters, L. B. Brubaker, and D. G. Gavin (2007), Understanding the origin and analysis of sediment-charcoal records with a simulation model, *Quaternary Science Reviews*, *26*, 1790-1809.

Higuera, P. E., L. B. Brubaker, P. M. Anderson, T. A. Brown, A. T. Kennedy, and F. S. Hu (2008), Frequent fires in ancient shrub tundra: implications of paleo-records for arctic environmental change, *PloS ONE*, *3*, e0001744, doi:10.137/journal.pone.0001744.

Higuera, P. E., L. B. Brubaker, P. M. Anderson, F. S. Hu, and T. A. Brown (2009), Vegetation mediated the impacts of postglacial climate change on fire regimes in the southcentral Brooks Range, Alaska, *Ecological Monographs*, *79*, 201-219.

Indermühle, A., T. F. Stocker, F. Joos, H. Fischer, H. J. Smith, M. Wahlen, B. Deck, D. Mastroianni, J. Tschumi, T. Blunier, R. Meyer, B. Stauffer (1999), Holocene carbon-cycle dynamics based on CO_2 trapped in ice at Taylor Dome, Antarctica. *Nature*, 398, 121-126.

Jacob, R., C. Schafer, I. Foster, M. Tobis, and J. Anderson (2001), Computational design and performance of the Fast Ocean Atmosphere Model: Version 1, in *The 2001 International Conference on Computational Science*, edited by V. N. Alexandrov, et al., pp. 175-184, Springer-Verlag.

Joussaume, S., and K. E. Taylor (2000), The Paleoclimate Modeling Intercomparison Project, in *Paleoclimate Modelling Intercomparison Project (PMIP): Proceedings of the Third PMIP Workshop*, edited by P. Braconnot, pp. 9-25.

Kerwin, M. W., J. T. Overpeck, R. S. Webb, and K. H. Anderson (2004), Pollen-based summer temperature reconstructions for the eastern Canadian boreal forest, subarctic, and Arctic, *Quaternary Science Reviews*, *23*, 1901-1924.

Lavoie, M., and P. J. H. Richard (2000), Postglacial water-level changes of a small lake in southern Québec, Canada, *The Holocene*, *10*, 621-634.

Leathwick, J. R., D. Rowe, J. Richardson, J. Elith, and T. Hastie (2005), Using multivariate adaptive regression splines to predict the distributions of New Zealand's freshwater diadromous fish, *Freshwater Biology*, *50*, 2034-2052.

Marti, O., P. Braconnot, J. Bellier, R. Benshila, S. Bony, P. Brockmann, P. Cadule, A. Caubel, S. Denvil, J. L. Dufresne, L. Fairhead, M. A. Filiberti, M.-A. Foujols, T. Fichefet, P. Friedlingstein, H. Goosse, J. Y. Grandpeix, F. Hourdin, G. Krinner, C. Lévy, G. Madec, I. Musat, N. de Noblet, J. Polcher, and C. Talandier (2005), The new IPSL Climate System Model: IPSL-Cm4.

Milborrow, S. (2009), earth: Multivariate Adaptative Regression Spline Models (R Package), edited by the Comprehensive R Archive Network (CRAN).

Miousse, L., N. Bhiry, and M. Lavoie (2003), Isolation and water-level fluctuations of Lake Kachishayoot, Northern Québec, Canada, *Quaternary Research*, *60*, 149-161.

Mitchell, T. D., and P. D. Jones (2005), An improved method of constructing a database of monthly climate observations and associated high-resolution grids, *International Journal of Climatology*, *25*, 693-712.

Moos, M. T., K. R. Laird, and B. F. Cumming (2009), Climate-related eutrophication of a

    small boreal lake in northwestern Ontario: a palaeolimnological perspective, *The*

    Holocene, *19*, 359-367.

Mudelsee, M. (2002), XTREND, a computer program for estimating trends in the

    occurrence rate of extreme weather and climate events, in *Scientific Reports*, edited by R.

    A. and K. Arnold, Institute of Meteorology, Institute for Tropospheric Research, Leipzig,

    Germany, pp. 149-195.

Mudelsee, M., M. Börngen, G. Tetzlaff, and U. Grünewald (2004), Extreme floods in central

    Europe over the past 500 years, Role of cyclone pathway "Zugstrasse Vb", *Journal of*

    Geophysical Research, *109*, D23101, doi: 10.1029/2004JD005034.

Muller, S. D., P. J. H. Richard, J. Guiot, J.-L. de Beaulieu, and D. Fortin (2003), Postglacial

    climate in the St. Lawrence lowlands, southern Québec: pollen and lake-level evidence,

    Palaeogeography, Palaeoclimatology, Palaeoecology, *193*, 51-72.

New, M., D. Lister, M. Hulme, and I. Makin (2002), A high-resolution data set of surface

    climate over global land areas, *Climate Research*, *21*, 1-25.

Overpeck, J. T., T. Webb III, and I. C. Prentice (1985), Quantitative interpretation of fossil

    pollen spectra: dissimilarity coefficients and the method of modern analogs, *Quaternary*

    Research, *23*, 87-108.

Payette, S., and L. Filion (1993), Holocene water-level fluctuations of a subarctic lake at the

    tree line in northern Québec, *Boreas*, *22*, 7-14.

Podur, J., D. L. Martell, and K. Knight (2002), Statistical quality control analysis of forest

    fire activity in Canada, *Canadian Journal of Forest Research*, *32*, 195-205.

Prentice, I. C., S. P. Harrison, D. Jolly, and J. Guiot (1998), The climate and biomes of Europe at 6000 yr BP: comparison of model simulations and pollen-based reconstructions, *Quaternary Science Reviews*, *17*, 659-668.

Ramstein, G., M. Kageyama, J. Guiot, H. Wu, C. Hély, G. Krinner, and S. Brewer (2007), How cold was Europe at the Last Glacial Maximum? A synthesis of the progress achieved since the first PMIP model-data comparison, *Climate of the Past*, *3*, 331-339.

Richardson, C. W. (1981), Stochastic simulation of daily precipitation, temperature, and solar radiation, *Water Resources Research*, *17*, 182-190.

Slingo, J. M., M. Blackburn, A. K. Betts, R. Brugge, B. J. Hoskins, M. J. Miller, L. Steenman-Clark, and J. Thuburn (1994), Mean climate and transience in the tropics of the UGAMP GCM. Part I: Sensitivity to convective parameterization, *Quarterly Journal of the Royal Meteorological Society*, *120*, 881-922.

Stocks, B. J., J. A. Mason, J. B. Todd, E. M. Bosch, B. M. Wotton, B. D. Amiro, M. D. Flannigan, K. G. Hirsch, K. A. Logan, D. L. Martell, and W. R. Skinner (2003), Large forest fires in Canada, 1959-1997, *Journal of Geophysical Research*, *108*, doi:10.1029/2001JD000484.

van Wagner, C. E. (1987), *Development and structure of the Canadian Forest Fire Weather Index System*, Forestry Technical Report No. 35, Canadian Forestry Service, Ottawa.

Vassiljev, S., S. P. Harrison, and J. Guiot (1998), Simulating the Holocene lake-level record of Lake Bysjön, southern Sweden, *Quaternary Research*, *49*, 62-71.

Viau, A. E., and K. Gajewski (2009), Reconstructing millennial-scale, regional paleoclimates of boreal Canada during the Holocene, *Journal of Climate*, *22*, 316-330.

Viau, A. E., K. Gajewski, M. C. Sawada, and P. Fines (2006), Millennial-scale temperature variations in North America during the Holocene, *Journal of Geophysical Research*, *111,* D09102, doi:10.1029/2005JD006031.

Yu, Y. Q., R. C. Yu, X. H. Zhang, and H. L. Liu (2002), A flexible coupled Ocean-Atmosphere General Circulation Model, *Advances in Atmospheric Sciences*, *19*, 169-190.

Yu, Z., and J. H. McAndrews (1994), Holocene water levels at Rice Lake, Ontario, Canada: sediment, pollen and plant-macrofossil evidence, *The Holocene*, *4*, 141-152.

Yu, Z., J. H. McAndrews, and D. Siddiqi (1996), Influences of Holocene climate and water levels on vegetation dynamics of a lakeside wetland, *Canadian Journal of Botany*, *74*, 1602-1615.

Yu, Z., J. H. McAndrews, and U. Eicher (1997), Middle Holocene dry climate caused by change in atmospheric circulation patterns: Evidence from lake levels and stable isotopes, *Geology*, *25*, 251-254.